https://doi.org/10.5194/acp-2021-201
Preprint. Discussion started: 11 March 2021

Atmospheric Chemistry and Physics Discussions
Open Access
EGU

Highly Oxygenated Organic Molecules Produced by the Oxidation of Benzene and Toluene in a Wide Range of OH Exposure and NO_x Conditions

Xi Cheng,[1] Qi Chen,[1,*] Yong Jie Li,[2,*] Yan Zheng,[1] Keren Liao,[1] Guancong Huang[1]

[1]State Key Joint Laboratory of Environmental Simulation and Pollution Control, BIC-ESAT and IJRC, College of Environmental Sciences and Engineering, Peking University, Beijing, China
[2]Department of Civil and Environmental Engineering, Faculty of Science and Technology, University of Macau, Taipa, Macau, China

**Correspondence to*: Qi Chen (qichenpku@pku.edu.cn) and Yong Jie Li (yongjieli@um.edu.mo)

Abstract. Oxidation of aromatic volatile organic compounds (VOCs) leads to the formation of tropospheric ozone and secondary organic aerosol, for which gaseous oxygenated products are important intermediates. We show herein experimental results of highly oxygenated organic molecules (HOMs) produced by the oxidation of benzene and toluene in a wide range of OH exposure and NO_x conditions. The results suggest multi-generation OH oxidation plays an important role in the product distribution, which likely proceeds more preferably via H subtraction than OH addition for early-generation products from light aromatics. Our experimental conditions promote the formation of more oxygenated products than previous flow-tube studies. The formation of dimeric products however was suppressed and might be unfavorable under conditions of high OH exposure and low NO_x in toluene oxidation. Under high-NO_x conditions, nitrogen-containing multifunctional products are formed, while the formation of other HOMs is suppressed. Products containing two nitrogen atoms become more important as the NO_x level increases, and the concentrations of these compounds depend significantly on NO_2. The highly oxygenated nitrogen-containing products might be peroxyacylnitrates, implying a prolonged effective lifetime of RO_2 that facilitates regional pollution. Our results call for further investigation on the roles of high-NO_2 conditions in the oxidation of aromatic VOCs.

https://doi.org/10.5194/acp-2021-201
Preprint. Discussion started: 11 March 2021

Atmospheric Chemistry and Physics Discussions

1 Introduction

Atmospheric oxidation of volatile organic compounds (VOCs) are crucial in the formation of tropospheric ozone (O_3) and secondary organic aerosol (SOA) (Calvert et al., 2015; Seinfeld and Pandis, 2016). Enormous studies have been conducted for the O_3 formation potentials and SOA yields of light aromatic VOCs such as benzene and toluene (Calvert et al., 2002; Atkinson and Arey, 2003; Ziemann and Atkinson, 2012). The peroxy radicals (either RO_2 or HO_2) that are generated from the oxidation process convert NO to NO_2. Ground-state oxygen atoms $O(^3P)$ are produced through the photolysis of NO_2, and the reaction between the $O(^3P)$ and O_2 is the main source of tropospheric O_3 (Calvert et al., 2015). The oxygenated organic products, on the other hand, may form SOA through either nucleation or condensation with various mass yields, depending on the structure of the precursors and the NO_x (= NO + NO_2) level (Ng et al., 2007; Li et al., 2016). Therefore, for both O_3 and SOA formation via VOC oxidation, NO_x plays critical roles (Atkinson, 2000; Sato et al., 2012; Tsiligiannis et al., 2019; Garmash et al., 2020).

OH-initiated oxidation of light aromatics occurs mainly via OH addition, with about 90% of preference (Calvert et al., 2002; Wu et al., 2014; Schwantes et al., 2017). As described in Sect. S1 in the Supplement, the formation of bicyclic peroxy radicals (BPRs) is central to aromatic oxidation in the absence of NO_x. Significant fractions of the oxidation (e.g., 0.35 for benzene and 0.65 for toluene) may lead to the formation of BPRs (Scheme S1 in the Supplement) (Birdsall et al., 2010), followed by further reactions to form highly oxygenated organic molecules (HOMs) (Crounse et al., 2013; Ehn et al., 2014; Berndt et al., 2016; Bianchi et al., 2019). The fate of the BPRs has been recently investigated by using time-of-flight chemical ionization mass spectrometer (TOF-CIMS), which is suitable for measuring HOMs. The TOF-CIMS measurements show that major products for the reactions between BPRs and HO_2/RO_2 in the absence of NO_x include carbonyls, alcohols, hydroperoxides, dimers, and alkoxy (RO) radicals (Birdsall et al., 2010; Wang et al., 2017; Molteni et al., 2018; Zaytsev et al., 2019; Garmash et al., 2020). The BPR-derived products that still possess the bicyclic skeleton are considered as the major ring-retaining products from the oxidation of light aromatics (Zaytsev et al., 2019). Decomposition of RO radicals may lead to fragmented products such as di-carbonyls and epoxides (Yu and Jeffries, 1997; Yu et al., 1997; Arey et al., 2009; Zaytsev et al., 2019). The formation of HOMs may involve multi-step auto-oxidation and multi-generation OH reaction (Zaytsev et al., 2019; Garmash et al., 2020; Y. Wang et al., 2020). Yet, it is still unclear whether the formation of HOMs is controlled by multi-step auto-oxidation or multi-generation OH oxidation.

Conditions of flow-tube or smog-chamber experiments have covered various conditions of OH concentrations (10^4 to 10^{11} molecule cm^{-3}) and residence times (10 s to 1 h) (Wang et al., 2017; Molteni et al., 2018; Garmash et al., 2020). Extrapolation of these results to tropospheric conditions requires further investigations under a wide range of NO_x levels. NO_x are rich in urban environments and compete with HO_2 and RO_2 for the termination of RO_2 radicals (Calvert et al., 2002; Seinfeld and Pandis, 2016). Early studies show a strong dependence of SOA mass yields on NO_x, owing to the formation of more-volatile products through the termination of RO_2 by NO (Ng et al., 2007; Sato et al., 2012). There are also a few recent studies on the gaseous oxygenated products from aromatic oxidation in the presence of NO_x (Tsiligiannis et al., 2019; Garmash et al., 2020; Y. Wang et al., 2020). Garmash et al. (2020) found that nitrated phenols (NPs) contribute significantly to the gaseous nitrogen-

https://doi.org/10.5194/acp-2021-201
Preprint. Discussion started: 11 March 2021

Atmospheric Chemistry and Physics
Discussions

containing HOMs produced by the benzene oxidation in the presence of NO_x. Tsiligiannis et al. (2019) show prevalent formation of organic nitrates (ONs) from 1,3,5-trimethylbenzene (TMB) oxidation, especially for atmospherically relevant $[NO_x]$:[VOC] ratios of greater than 1. In addition to ONs, Y. Wang et al. (2020) show the elevated formation of dinitrates from the oxidation of TMB isomers in the presence of NO_x. In general, the formation of these nitrogen-containing products suppresses the formation of other HOMs (Tsiligiannis et al., 2019; Garmash et al., 2020; Y. Wang et al., 2020). However, the dependence of product distributions on NO_x conditions (e.g., $[NO_x]$:[VOC] or $[NO_2]$:[NO] ratios) remains largely unclear.

In this study, we investigate the production of gaseous HOMs from the OH-initiated oxidation of benzene and toluene in an oxidation flow reactor (OFR) by using nitrate-adduct TOF-CIMS (NO_3^--TOF-CIMS). A wide range of OH exposure and NO_x conditions are studied. Distributions and molar yields of key products are investigated. Kinetic analysis helps inferring the possible formulas of nitrogen-containing HOMs.

2 Experimental Section

2.1 Oxidation flow reactor

The oxidation experiments are conducted in a 13.3-L Aerodyne Potential Aerosol Mass (PAM) OFR reactor. The schematic of the experimental setup and the example experimental sequence are shown in Figs. S1 and S2 in the Supplement, respectively. The OFR was operated in two continuous-flow modes named as OFR254-5 and OFR254-5-iN_2O (Lambe et al., 2017; Peng et al., 2018). For the OFR254-5 mode, the inside UV lamps emit photons at 254 nm to generate OH radicals in the reactor via the reaction of $O(^1D) + H_2O \rightarrow 2OH$. An outside UV lamp produces O_3 and leads to about 5 ppm of O_3 in the OFR. For the OFR254-5-iN_2O mode, N_2O (99.5%) is injected into the OFR to achieve N_2O mixing ratios of 1.1% (OFR254-5-iN_2O1.1) and 4.4% (OFR254-5-iN_2O4.4). NO and NO_2 are then formed by the reaction $O(^1D) + N_2O \rightarrow 2NO$, followed by the reaction $NO + O_3 \rightarrow NO_2 + O_2$ (Lambe et al., 2017). The conditions for OFR254-5 are considered as low-NO_x, whereas the latter are high-NO_x. Under each of these three sets of experiments, OH exposure and NO_x levels were varied by ramping the voltage of the UV lamps in the OFR. The total flow rate was about 8.4 L min^{-1}, resulting in a mean residence time of 95 s in the OFR. Relative humidity (RH) in the OFR was about 20 to 55% at 25 ± 2 °C, corresponding to H_2O mixing ratios of about 0.7 to 1.5%. Details about the experimental setup are provided in Sect. S2 in the Supplement.

In total, 28 experiments were conducted for initial mixing ratios of 110 ppb benzene and 50 ppb toluene. Table S1 in the Supplement lists the experimental conditions as well as measured and derived quantities for all experiments. The concentrations of reactive species such as OH, HO_2, NO, and NO_2 were estimated by an OFR-based photochemical box model (PAMchem) (Lambe et al., 2017). The box model simulations are described in detail in Sect. S2, for which calibration experiments with SO_2 was conducted to constrain the actinic flux at 254 nm (Fig. S3 in the Supplement). Briefly, the model suggests OH exposure of about 1.1×10^{11} to 2.5×10^{12} molecules cm^{-3} s for our experiments, corresponding to equivalent photochemical age of 0.8 to 19.3 days with a mean OH concentration of 1.5×10^6 molecules cm^{-3}. For high NO_x experiments,

https://doi.org/10.5194/acp-2021-201
Preprint. Discussion started: 11 March 2021

the OFR-exit NO and NO_2 concentrations were 0.2 to 5.1 ppb and 15.8 to 231.4 ppb, respectively, leading to $[NO_x]$:[VOC] ratios of 0.2 to 2.2 for benzene and 0.4 to 4.7 for toluene.

2.2 Chemical characterization

HOMs were characterized by an Aerodyne NO_3^--TOF-CIMS. Details about the instrument operation and data analysis are described elsewhere (Cheng et al., 2020). Briefly, mass calibration was performed on the reagent ions and selected Teflon-related ions, which covers the *m/z* range of 62 to 676 with mass accuracies of less than 10 ppm. The "non-production" ions were identified by positive matrix factorization (PMF) analysis and were removed from the analysis (Fig. S4 in the Supplement). The $HNO_3NO_3^-$-adduct ions were identified by the signal correlations between the NO_3^--adduct and $HNO_3NO_3^-$-adduct ions and were removed from the analysis (Fig. S5 in the Supplement). Only NO_3^- adduct ions are presented herein. The background signals of individual ions were determined on the basis of the measurements made without the injection of VOCs (Fig. S2). Because of the lack of standards, we applied the calibration factor of 4-nitrophenol (i.e., 0.0020 ncps ppt^{-1} or 1.66×10^{10} molecules cm^{-3}) to HOMs, which is similar to the commonly-used calibration factors of H_2SO_4 (i.e., 1.62×10^{10} molecules cm^{-3} for our instrument herein and 1.89×10^{10} molecules cm^{-3} reported by Jokinen et al. (2012)) and perfluoroheptanoic acid (i.e., 1.6×10^{10} molecules cm^{-3} reported by Ehn et al. (2014)). All calibration factors are corrected by wall loss. Ehn et al. (2014) reported a ± 50% of uncertainty. For our experiments, we estimate an uncertainty of 42% on the basis of nitrated phenol calibrations (Cheng et al., 2020). In some experiments, the VOC precursors and less-oxygenated gaseous products were monitored by an IONICON proton transfer reaction-quadrupole interface time-of-flight mass spectrometer (PTR-QiTOF). The instrument operation and data analysis have been described previously (Huang et al., 2019). The measurements have a total uncertainty of about 21%. Particle size distributions were measured by a scanning mobility particle sizer (SMPS, TSI, 3938). The SOA mass concentrations are measured by an Aerodyne long-time-of-flight soot-particle aerosol mass spectrometer (LTOF-SP-AMS) (Zheng et al., 2020).

3 Results and discussion

3.1 Product categories

Figure 1 shows the mass spectra of gaseous oxygenated products produced by benzene and toluene oxidation in typical low- and high-NO_x experiments. The fitted ion peaks are categorized into fragmented products, open-shell products, closed-shell products, and dimeric products as well as nitrogen-containing products when NO_x is present. Tables S2-S3 in the Supplement list the corresponding peak lists and relative signal contributions of major products in each category. The fragmented products are the most abundant category under low-NO_x conditions. They have carbon numbers less than their precursors, indicating possibly ring opening/scission from presumably RO radicals (Zaytsev et al., 2019). $C_2H_4O_4$ shows the highest signal intensity in the fragmented category under low-NO_x conditions. $C_4H_4O_5$ and $C_5H_4O_6$ are the other two abundant common products in this category. Under high-NO_x conditions, $C_4H_2O_5$ is the most abundant common product for benzene and toluene oxidation. Many of the fragmented products have been detected in SOA (Gallimore et al., 2011; Gowda and Kawamura, 2018).

The ring-retaining HOM products may have even (closed-shell) or odd (open-shell) hydrogen numbers (Molteni et al., 2018; Zaytsev et al., 2019; Garmash et al., 2020). The open-shell products observed by the NO_3^--TOF-CIMS are more likely RO_2 radicals rather than RO radicals because that with relatively large carbon numbers, the former have lifetimes of seconds that are much longer than the latter of < 10^{-4} s (Orlando et al., 2003; Seinfeld and Pandis, 2016; Zhao et al., 2018). Under low-NO_x conditions, the BPRs (i.e., $C_6H_7O_5$ from benzene oxidation and $C_7H_9O_5$ from toluene oxidation) have relatively low signal intensities (0.1%). Products that are presumably formed by further auto-oxidation of BPRs such as $C_6H_7O_7$ and $C_6H_7O_9$ for benzene (or $C_7H_9O_7$ and $C_7H_9O_9$ for toluene) have much greater signal intensities compared with the BPRs, especially for the O_9 products. Other open-shell products with two less hydrogen atoms (e.g., H_5 for benzene and H_7 for toluene) or with an even number of oxygen atoms (e.g., O_6 or O_{10}) are also present. Under high-NO_x conditions, the main open-shell products are the O_9 products, similar to the low-NO_x case.

Among the closed-shell products produced by benzene oxidation, $C_6H_6O_{5-10}$ and $C_6H_8O_{5-10}$ with one oxygen atom apart show relatively high signal intensities, and $C_6H_6O_5$ and $C_6H_6O_6$ are the most abundant ones. $C_6H_6O_5$ and $C_6H_6O_6$ might be carbonyl products from the termination of $C_6H_7O_6$ and $C_6H_7O_7$ by HO_2 or RO_2 (Zaytsev et al., 2019; Garmash et al., 2020). $C_6H_7O_6$ is probably formed by the ring breakage of bicyclic alkoxy radical followed by the 1,5 aldehydic alkoxy H-shift reactions (Xu et al., 2020), which involves the RO pathway as described in detail in Sect. S3 of the Supplement. For other products formed by the termination reactions of BPR with HO_2 or RO_2, bicyclic hydroperoxide ($C_6H_8O_5$), carbonyl ($C_6H_6O_4$) and alcohol ($C_6H_8O_4$) have relatively small signals, whereas the products that may involve two or three steps of auto-oxidation (e.g., $C_6H_8O_7$ and $C_6H_8O_9$) have greater signal intensities. Similarly for toluene oxidation, the bicyclic hydroperoxide ($C_7H_{10}O_5$) shows lower signals than $C_7H_{10}O_7$ and $C_7H_{10}O_9$ that may be associated with multiple steps of auto-oxidation. $C_7H_8O_6$ and $C_7H_8O_7$ are the main closed-shell products that might be carbonyls that are produced by the termination of $C_7H_9O_7$ and $C_7H_9O_8$ by HO_2 or RO_2, respectively. The formation of $C_7H_8O_7$ may also be explained by the RO pathway, similar to $C_6H_6O_5$ (Sect. S3). The RO pathway, if it occurs, may potentially lead to various products with significant signals, which remains largely overlooked in studies of aromatic oxidation (Xu et al., 2020).

The other two categories are dimeric and nitrogen-containing products. Under low-NO_x conditions, dimeric products with 8-14 even oxygen atoms are clearly present. $C_{12}H_{14}O_8$ and $C_{14}H_{18}O_8$ are perhaps formed via self-reactions of the BPRs for benzene and toluene, respectively. The distribution of dimeric products is in line with the open-shell and closed-shell products. We observe a number of dimeric products with odd oxygen numbers that are perhaps produced by cross-reactions of odd- and even-oxygen RO_2 (Molteni et al., 2018; Garmash et al., 2020). The presence of NO_x results in the formation of nitrogen-containing products with one or two nitrogen atoms, and the signal abundances of all other oxygenated products are much lower than the case of low-NO_x experiments. Such a suppression has been reported previously (Tsiligiannis et al., 2019; Garmash et al., 2020; Y. Wang et al., 2020; Mehra et al., 2020). The nitrogen-containing products are expected to be organic

https://doi.org/10.5194/acp-2021-201
Preprint. Discussion started: 11 March 2021

nitrates or nitrated phenols. For benzene oxidation, $C_6H_5NO_3$, $C_6H_5NO_4$, and $C_6H_4N_2O_6$ are the most abundant, which are plausibly nitrophenol, nitrocatechol, and dinitrocatechol, respectively. For toluene, $C_6H_5NO_3$ (nitrophenol), $C_6H_5NO_4$ (nitrocatechol), $C_7H_7NO_3$ (methylnitrophenol), and $C_7H_7NO_4$ (methylnitrocatechol) are the main tentatively assigned nitrated phenols. Significant secondary production of these compounds from aromatic oxidation have been observed in urban Beijing (Cheng et al., 2020). Other products such as $C_6H_7NO_8$, $C_6H_7NO_9$, and $C_7H_9NO_8$ are most likely organic (peroxy) nitrates. Scheme S2 in the Supplement gives an example of proposed formation mechanisms for nitrogen-containing products starting from the BPR of $C_7H_9O_5$.

3.2 Low-NO_x conditions

Product Distribution. The products that we observed herein (Tables S2-S3) are generally in agreement with those found in previous low-NO_x studies (Schwantes et al., 2017; Molteni et al., 2018; Zaytsev et al., 2019; Mehra et al., 2020; Garmash et al., 2020). Differences exist in the relative abundance of species with different oxygen contents within each product category (Molteni et al., 2018; Garmash et al., 2020). Table S4 in the Supplement lists the experimental conditions and relative signal intensities of some major oxygenated products formed by benzene oxidation. Molteni et al. (2018) observes predominant production of $C_6H_8O_5$ (plausibly hydroperoxides) and $C_{12}H_{14}O_8$. Garmash et al. (2020) shows relatively high signals of $C_6H_8O_9$ and $C_{12}H_{14}O_8$, whereas the chamber study and our study both show relatively high signals of $C_6H_8O_7$ and $C_6H_8O_9$ and lower signals of dimeric products. Moreover, the signal intensities of RO_2 (e.g., $C_6H_7O_5$ and $C_6H_7O_7$) are greater in our study than in other studies. Both experimental conditions and instrument detection are factors that may affect the product distribution. For example, a longer residence time might promote multi-step auto-oxidation. For auto-oxidation, H shift has rate constants of about 10^{-3} to 1 s^{-1} and is likely the rate-determining step under atmospheric conditions, having reaction times of 1 to 10^3 s that are much longer than the subsequent O_2 addition of μs (Orlando et al., 2003; Bianchi et al., 2019). Garmash et al. (2020) indicated that fewer auto-oxidation steps would be expected in flow-tube experiments. The flow-tube study herein has relatively longer residence time than others, which is consistent with relatively more abundant O_7 and O_9 products. Ambient environments have much lower OH concentrations but longer residence times depending on meteorological conditions, which may suggest more oxygenated products from multi-steps of auto-oxidation. For detection, the instrument efficiency might be different for HOMs having different clustering capability (e.g., numbers of functional group as hydrogen-bond donors) (Hyttinen et al., 2015). Tuning might affect the transmission of product ions in different *m*/*z* range or affect the efficiency of dimer clustering (Heinritzi et al., 2016; Brophy and Farmer, 2015).

Effects of OH Exposure. As shown in Fig. 2a, the concentrations of fragmented, closed-shell, open-shell and dimeric products formed by benzene oxidation increase with increasing OH exposure that corresponds to 2.4 to 16.1 days of atmospheric equivalent photochemical age. Elevated concentrations of open-shell products (e.g., RO_2) and HO_2 are expected for greater OH exposure, leading to enhanced production of the closed-shell and dimeric products through the $RO_2 + HO_2$ and $RO_2 + RO_2$ reactions. These processes may be limited by the availability of RO_2 (< 0.9 ppt in our study) rather than that of HO_2 (0.5 - 2.4

https://doi.org/10.5194/acp-2021-201
Preprint. Discussion started: 11 March 2021

ppb) (Table S1). Consistently, the concentrations of dimeric products are much lower than that of monomeric closed-shell products. For toluene oxidation, the dependence of the product formation on OH exposure is less significant than that for benzene (Fig. 2b). The concentrations of fragmented, closed-shell and open-shell products first increase and then slightly decrease with the increasing OH exposure that corresponds to 2.4 to 19.4 days of atmospheric equivalent photochemical age. Interestingly, the concentrations of dimeric products decrease as the OH exposure increases, suggesting unfavorable dimer formation under conditions of high OH exposure for toluene oxidation. Whether this phenomenon is related to the substituted methyl group or not needs further investigations. The overall atomic oxygen-to-carbon (O:C) ratios of HOM products increase from 1.18 to 1.26 for benzene oxidation and from 1.16 to 1.23 for toluene oxidation as the OH exposure increases, suggesting more oxygenated product distributions as detected. The overall atomic hydrogen-to-carbon (H:C) ratios of HOMs are 1.10-1.14 for benzene oxidation and 1.14-1.18 for toluene oxidation, and the changes with OH exposure are negligible.

Figure 2c-d shows the concentrations of individual representative open-shell and closed-shell products for increasing OH exposures. The open-shell products are mainly $C_xH_{y+1}O_5$ (BPRs) and $C_xH_{y+1}O_7$ (RO_2 formed from one more step of auto-oxidation). The concentrations of $C_xH_{y+1}O_7$ are approximately one order of magnitude higher than the concentrations of $C_xH_{y+1}O_5$. The closed-shell products such as hydroperoxides ($C_xH_{y+2}O_{5,7}$), carbonyls ($C_xH_yO_{4,6}$), and alcohols ($C_xH_{y+2}O_{4,6}$) may be differentiated by the numbers of hydrogen and oxygen in the molecular formulas (Mentel et al., 2015; Molteni et al., 2019). Specifically, the products with two more hydrogen atoms than the precursor should be hydroperoxides ($C_xH_{y+2}O_z$) if z is an odd number and alcohols if an even number considering multiple steps of auto-oxidation for BPRs or RO_2 radicals. On the other hand, products that have the same hydrogen atoms ($C_xH_yO_z$) should be carbonyls with an even number of z, or if the carbonyl formation involves the RO pathway, $C_xH_yO_z$ with an odd number of z can be formed. The concentrations of $C_xH_{y+2}O_7$ and $C_xH_yO_6$ originated from $C_xH_{y+1}O_7$ are 1 to 2 orders of magnitudes greater than the concentrations of $C_xH_{y+2}O_5$ and $C_xH_yO_4$ originated from $C_xH_{y+1}O_5$. The greater signals of O_7 products suggest our experimental conditions perhaps favor the formation of more-oxygenated products.

Enhanced formation of more oxygenated products was observed for elevated OH exposures. For example, the concentrations of $C_6H_7O_7$ increase first and stay relatively stable as the OH exposure increases, whereas the concentrations of $C_6H_7O_5$ decreases at high OH exposures for benzene oxidation. The concentrations of the hydroperoxide products ($C_xH_{y+2}O_{5,7}$) such as $C_6H_8O_7$ increases as OH exposure increases whereas the concentrations of $C_6H_8O_5$ decreases. For toluene oxidation, the concentrations of $C_xH_{y+2}O_{5,7}$ ($C_7H_{10}O_5$ and $C_7H_{10}O_7$) both decrease. The concentrations of carbonyl products ($C_xH_yO_{4,6}$) increase with OH exposure for benzene but not for toluene. We do not observe significant signals for $C_xH_{y+2}O_4$ (alcohols) from BPR $C_xH_{y+1}O_5$, but $C_xH_{y+2}O_6$ from RO_2 $C_xH_{y+1}O_7$ are of high concentrations. The concentrations of $C_6H_8O_6$ (alcohol) from benzene also increase as the OH exposure increases while the concentrations for $C_7H_{10}O_6$ from toluene decrease. Overall, the enhanced formation of more-oxygenated products at high OH exposure is more significant for benzene than for toluene. A possible explanation is that toluene oxidation may involve more multi-generation OH oxidation because of the substituted methyl group.

https://doi.org/10.5194/acp-2021-201
Preprint. Discussion started: 11 March 2021

Atmospheric Chemistry and Physics Discussions

Increasing OH exposure also enhances the formation of more-oxygenated fragmented products (Fig. S6 in the Supplement). $C_4H_4O_3$ (perhaps epoxybutanedial) has been widely observed in aromatic oxidation (Wang et al., 2013; Wu et al., 2014; Zaytsev et al., 2019). The concentrations of $C_4H_4O_3$ decrease monotonically as the OH exposure increases for both benzene and toluene oxidation. For toluene oxidation, $C_3H_4O_2$ (perhaps methylglyoxal), $C_4H_4O_2$ (perhaps butenedial) and $C_5H_6O_2$ (perhaps methylbutenedial) that were detected by the PTR-QiTOF also show similar monotonic decreases. By contrast, the concentrations of $C_3H_4O_5$, $C_4H_4O_5$, and $C_5H_4O_6$ increase with increasing OH exposures for both benzene and toluene oxidation. The concentrations of other $O_{5\text{-}7}$ products also increase as the OH exposure increases. Similar to the open-shell and closed-shell products, the increasing trends are more significant for benzene-derived products than those for toluene-derived ones. This observation is in agreement with Garmash et al. (2020) who suggested that first-generation fragmented products were converted to more-oxygenated ones through further oxidation as the OH exposure increases. Alternatively, these more-oxygenated fragmented products might also be direct decomposition products of highly oxygenated RO radicals, which have been shown to play important roles in product formation (Noda et al., 2009; Birdsall and Elrod, 2011).

Multi-generation OH oxidation. Because of high OH exposures, the OFR conditions usually favor multi-generation reactions (Lambe et al., 2011). Products with hydrogen numbers < y and > y+2 may be produced by multi-generation OH reactions. For example, the closed-shell products from benzene oxidation should contain at least one double bond which can further react with OH radicals via OH addition to form products with two more hydrogen atoms (e.g., to form $C_6H_{10}O_z$). The formation of $C_6H_4O_z$ from the closed-shell products of benzene oxidation may involve multi-generation OH reactions via H abstraction and subsequent termination by a loss of OH or HO_2 (Molteni et al., 2018; Garmash et al., 2020). There are significant contributions of products with hydrogen numbers < y and > y+2 in our experiments (Tables S2 and S3), highlighting the importance of multi-generation OH reactions in production formation. On the other hand, the formation of y and y+2 products may also involve multi-step OH addition or H subtraction that make conversions between the two groups of products. For the phenolic pathway, the main products of $C_6H_6O_z$ and $C_7H_8O_z$ may be produced by dihydroxy-, trihydroxy- and even multi-OH substituted-benzene or toluene (Schwantes et al., 2017).

Figure 3 shows the concentrations and the relative contributions of the closed-shell product groups including $C_xH_{y-2}O_z$, $C_xH_yO_z$, $C_xH_{y+2}O_z$ and $C_xH_{y+4}O_z$. For both benzene and toluene oxidation, the concentrations of these closed-shell products increase as the OH exposure increases for the atmospherically relevant equivalent photochemical age (< 10 days). For greater OH exposures, the concentrations of y-2 products keep increasing, whereas the concentrations of other products start to decrease (Fig. 3a-b). The decreasing trends at high OH exposures are more significant for toluene-derived products. Such differences might be explained by the methyl group in toluene and the added -OH groups during oxidation. Both functional groups increase the electron density on the aromatic ring through a resonant electron-donating effect, thereby activating the aromatic ring and facilitating further addition reactions to form products with multiple -OH groups (M. Wang et al., 2020). Interestingly, the relative fractions of the $C_xH_{y-2}O_z$ and $C_xH_{y+4}O_z$ products for both benzene and toluene oxidation show opposite trends (Fig. 3c-d). The increasing fractions of y-2 products but decreasing fractions of y+4 products for increasing OH exposures as well as

https://doi.org/10.5194/acp-2021-201
Preprint. Discussion started: 11 March 2021

the monotonically increasing concentration of *y*-2 products suggest that the multi-generation OH oxidation may proceed preferably via H subtraction rather than OH addition. Compared with their precursors (benzene and toluene), the closed-shell products are less conjugated and thus OH addition is probably less favorable.

Estimated Molar Yields. Figure S7 in the Supplement shows the scatter plot of the concentrations of HOMs detected by NO_3^--TOF-CIMS and the VOC oxidation rate for benzene and toluene oxidation under low-NO_x conditions. As expected, the product concentrations increase with the VOC oxidation rates. Our estimated molar yields for the HOM products are 0.22 ± 0.10% (mean ± one standard deviation) for benzene oxidation and 0.46 ± 0.20% for toluene oxidation (Sect. S4). These yields are much lower than the smog-chamber results of 4.1% to 14.0% for benzene oxidation reported by Garmash et al. (2020) but slightly greater than the flow-tube yields of 0.1% to 0.2% reported by Molteni et al. (2018). A key difference of the experimental conditions is the much longer residence time in the chamber study (Table S4), suggesting perhaps a long characteristic time of HOM formation from aromatic oxidation. Instrument sensitivity might also affect the detection of HOMs but less likely lead to orders of magnitude difference in yields.

3.3 High-NO_x conditions

Effects of NO_x Level. The NO or NO_2 termination of RO_2 radicals competes with the HO_2 or RO_2 termination and forms nitrogen-containing species at the expense of other highly oxygenated products (Tsiligiannis et al., 2019; Garmash et al., 2020; Y. Wang et al., 2020; Mehra et al., 2020). Yet, quantitative understanding in the effects of NO_x on the formation of oxygenated products is limited for aromatic precursors compared with those for biogenic VOCs (Nah et al., 2016; Lambe et al., 2017; Sarnela et al., 2018). The high-NO_x experiments herein were conducted with $[NO_2]$:[NO] ratios of 20 to 120 (Table S1), which may represent urban afternoon conditions when fresh NO_x emission is mostly converted to NO_2 and intense photochemistry fuels the oxidation of aromatics accompanying the NO_x emission (Newland et al., 2021). Figure 4 shows the concentrations of observed HOMs for various $[NO_x]$:$[HO_2]$ conditions. We use $[NO_x]$:$[HO_2]$ instead of [NO]:$[HO_2]$ to evaluate termination pathways to form various nitrogen-containing products such as nitrated phenols, organic nitrate, and peroxynitrate. The contributions from RO_2 + RO_2 termination are probably minor because of the low concentrations of RO_2 (< 0.9 ppt). Given the low and narrow range of NO_x levels in the OFR254-iN_2O1.1 experiments, the product concentrations for all lamp voltages (i.e., a range of OH exposure) are averaged and shown as the first data point in each panel of Fig. 4.

Similar to previous findings, nitrogen-containing products are the dominant species in the spectra with concentrations up to 18.3 and 7.3 ppt for benzene and toluene oxidation, respectively. The concentrations of all HOMs start to decrease at high $[NO_x]$:$[HO_2]$ ratios, except that the concentrations of dimeric products from benzene oxidation remain steady (Fig. 4a-b). The decreasing trends for closed-shell, open-shell, and fragmented products are expected, indicating significant competition of radical terminations by NO or NO_2. The decreasing concentrations of nitrogen-containing products for increasing $[NO_x]$:$[HO_2]$ are however counterintuitive. Figure 4c-d shows the concentrations of main individual nitrogen-containing products. The initial increase of the concentrations of nitrogen-containing species might be explained by a decrease of HO_2 concentrations from 0.8

https://doi.org/10.5194/acp-2021-201
Preprint. Discussion started: 11 March 2021

Atmospheric Chemistry and Physics Discussions

- 1.5 ppb to 0.5 - 0.7 ppb as a result of the switch of 1.1% of N_2O injection to 4.4% (Table S1). The further reduction of these compounds as [NO_x]:[HO_2] increases is probably related to the simultaneous decrease of RO_2, or alternatively further reactions to products that have two nitrogen atoms. Figure S8 in the Supplement shows similar concentration trends for individual ring-scission and ring-retaining products with or without nitrogen in their formulas. There seems to be "optimal" [NO_x]:[HO_2] ratios of 130 to 240 for the formation of nitrogen-containing products. The dependence of those products with only one nitrogen atom on NO_x is however not strong. The availability of RO_2 is perhaps the key factor that limits their formation at low NO_x levels and affects further reactions to form products with two nitrogen atoms at high NO_x levels.

Nitrated phenols are the most abundant nitrogen-containing products under high-NO_x conditions. In aromatic oxidation, these compounds are formed by the reaction of phenoxy RO radicals with NO_2 (Jenkin et al., 2003). In the Master Chemical Mechanism (MCM v3.3.1), the phenoxy RO radicals can be formed via OH oxidation of phenols (k_{OH} = 2.8 × 10^{-11} cm^3 molecule s^{-1}) with a low branching ratio of 0.06. They can also be formed by the NO_3 oxidation of phenols (k_{NO_3} = 3.8 × 10^{-12} cm^3 molecule s^{-1}) with a high branching ratio of 0.74 (IUPAC, 2008). Under high-NO_x conditions, the estimated concentrations of OH and NO_3 radicals are 0.05 to 0.3 ppb and 0.01 to 0.09 ppb, respectively, suggesting that the NO_3 oxidation of phenols contributed efficiently to the formation of nitrated phenols in the OFR experiments herein. When [NO_x]:[HO_2] increases, the concentrations of $C_{6,7}H_{5,7}NO_4$ (perhaps nitrocatechol or methylnitrocatechol) increase first and then decrease. The concentrations of $C_{6,7}H_{5,7}NO_3$ (perhaps nitrophenol or methylnitrophenol) however show a weak dependence on the NO_x level, suggesting the availability of RO radical might be the limiting factor in controlling the formation of nitrated phenols herein. Interestingly, the concentrations of products with two nitrogen atoms such as $C_6H_4N_2O_6$, $C_6H_8N_2O_9$, and $C_7H_{10}N_2O_9$ (only for toluene) steadily increase as [NO_x]:[HO_2] rises, suggesting a strong dependence of the formation of these species on NO_2.

Formation of ROOH, RONO$_2$, and ROONO$_2$. Jenkin et al. (2019) suggested that the overall rate coefficients for RO_2 + HO_2 reactions are 1.92 × 10^{-11} and 1.98 × 10^{-11} cm^3 $molecules^{-1}$ s^{-1} at 298 K for benzene and toluene oxidation, respectively. For the OFR conditions (Table S1), the characteristic time for the RO_2 termination by HO_2 was perhaps < 10 s, which is much shorter than the OFR residence time of 95 s. The rate coefficients of the hydroperoxide pathway ($RO_2 + HO_2 \rightarrow ROOH + O_2$) may be constrained by the concentration ratios of [ROOH] multiplied by the loss rate of ROOH to [RO_2][HO_2] (Sect. S5 in the Supplement). For example, assuming that the $C_6H_7O_7$ and $C_7H_9O_7$ are the RO_2 radicals, and $C_6H_8O_7$ and $C_7H_{10}O_7$ are the corresponding ROOH for benzene and toluene oxidation, respectively, the slopes in Fig. 5a indicate that the rate coefficients of hydroperoxides are 1.20 × 10^{-11} and 1.26 × 10^{-11} cm^3 $molecules^{-1}$ s^{-1}. These rate coefficients suggest that the branching ratios of the hydroperoxide formation under low-NO_x conditions are 0.62 and 0.64 for benzene- and toluene-derived RO_2, respectively, which are consistent with the estimated branching ratios of 0.52 - 1.00 in literature (Jenkin et al., 2019).

In the presence of NO_x, the reactions between $C_xH_{y+1}O_7$ and nitrogen oxides lead to both chain propagation and chain termination to form RO radicals and nitrogen-containing products. Similar to the analysis of the hydroperoxide formation, the slopes in Fig. 5b suggest that the rate coefficients of $RO_2 + NO(+M) \rightarrow RONO_2(+M)$ are 2.87 × 10^{-11} and 6.12 × 10^{-11} cm^3 $molecules^{-1}$ s^{-1} for benzene and toluene oxidation under OFR254-5-iN_2O1.1 conditions, respectively (Sect. S5). These

https://doi.org/10.5194/acp-2021-201
Preprint. Discussion started: 11 March 2021

coefficients are more than one order of magnitude greater than the values reported by Jenkin et al. (2019) (i.e., 8.09×10^{-13} and 1.10 - 8.45×10^{-13} cm^3 $molecules^{-1}$ s^{-1} for benzene and toluene oxidation, respectively). One explanation is that the detected $C_xH_{y+1}NO_8$ contains multifunctional groups and represents not only non-peroxy organic nitrates ($RONO_2$) but also peroxy organic nitrates ($ROONO_2$). As shown in Fig. 5c, the $[C_xH_{y+1}NO_8]$:$[C_xH_{y+2}O_7]$ ratios start to decrease at higher [NO]:$[HO_2]$ in our OFR254-5-iN_2O4.4 experiments. The competition between NO and HO_2 for terminating RO_2 should not alter the rate coefficients and the branching ratios (Atkinson and Arey, 2003). The lack of linear relationship of $[C_xH_{y+1}NO_8]$:$[C_xH_{y+2}O_7]$ (i.e., assumed as $[RONO_2]$:[ROOH]) on [NO]:$[HO_2]$ ratio is consistent with the possibility of $C_xH_{y+1}NO_8$ partially being $ROONO_2$, especially for toluene oxidation.

Xu et al. (2020) indicate that the formation of non-peroxy organic nitrates ($RONO_2$) is minor in aromatic oxidation. The detected $ROONO_2$ are likely RC(O)$OONO_2$, because that $ROONO_2$ are usually thermally unstable intermediates (Kirchner et al., 1999) and RC(O)$OONO_2$ can be detected by the NO_3^--TOF-CIMS (Rissanen, 2018). Acylperoxy radicals RC(O)OO (i.e., a type of peroxy radical) may react with NO_2 to produce peroxyacylnitrate (RC(O)$OONO_2$) (Jenkin et al., 2019). The formation of the RC(O)$OONO_2$ requires (1) the original RO_2 radicals to be $C_xH_{y+1}O_6$ instead of $C_xH_{y+1}O_7$ and (2) an acyl (-C=O) group that is connected to the O-O bond. The formation of $C_xH_{y+1}O_6$ is feasible through the RO pathway (Sect. S3). The hydroperoxides corresponding to $C_xH_{y+1}O_6$ are $C_xH_{y+2}O_6$ (i.e., $C_6H_8O_6$ and $C_7H_{10}O_6$ for benzene and toluene, respectively). Figure 5d-e shows the increase of $[C_xH_{y+1}NO_8]$:$[C_xH_{y+2}O_6]$ (i.e., perhaps [RC(O)$OONO_2$]:[ROOH]) for increasing $[NO_2]$:$[HO_2]$ ratios. In particular, the relationship between $[C_xH_{y+1}NO_8]$:$[C_xH_{y+2}O_6]$ and $[NO_2]$:$[HO_2]$ is nearly linear at high $[NO_2]$:$[HO_2]$ ratios in the OFR254-5-iN_2O4.4 experiments. There is a lack of kinetic data for the reactions of RC(O)OO + NO_2 (Rissanen, 2018), which prevents us from further investigation.

4 Atmospheric Implications

In this study, we investigated the formation of HOMs in the OFR by the oxidation of benzene and toluene in a wide range of OH exposure and NO_x conditions. The results show enhanced formation of more-oxygenated products for elevated OH exposures. The formation of dimeric products however seems unfavorable under conditions of high OH exposure and low NO_x for substituted aromatics. The suppression of dimeric products may affect the contribution of aromatic HOMs to new particle formation in the downwind of urban atmosphere. The changes of product distribution and concentration also suggest that multi-generation OH oxidation may proceed preferably via H subtraction rather than OH addition. For aged air masses, this may reduce the H:C ratios of HOM products from aromatic oxidation. Under high-NO_x conditions, we show that the formation of products containing one nitrogen atom perhaps depend more significantly on the organic radicals (RO or RO_2) but less so on NO_2, while formation of products containing two nitrogen atoms depends significantly on NO_2. Further investigation on the roles of high-NO_2 conditions that represent a wide range of anthropogenically influenced environments in the oxidation of aromatic VOCs are needed. Moreover, we found that non-peroxy organic nitrates might form via RO_2 + NO under low-NO_2 conditions; and RO_2 + NO_2 may dominate to produce $ROONO_2$ or RC(O)$OONO_2$ under high-NO_2 conditions. The reaction of

RC(O)OO with NO_2 to produce peroxyacylnitrates should be of particular importance with high $[NO_2]$:[NO] ratios of tens to hundreds. Both of $ROONO_2$ and $RC(O)OONO_2$ are reservoirs of RO_2 radicals. Under conditions of high $[NO_2]$:[NO] ratios (e.g., late afternoon in urban or suburban environments), the "effective" lifetimes of RO_2 radicals might become longer because of the formation of $RC(O)OONO_2$. Subsequent slow release of RO_2 radicals with the help of NO_2 may extend the formation of HOMs from VOC oxidation in urban environments to early evening when OH starts to decline and NO_3 has not yet built up, facilitating the development of regional SOA pollution.

Data availability. Data presented in this manuscript are available upon request to the corresponding author.

Author contributions. QC and YJL designed the study. XC conducted the experiments and data analysis with the help of YZ, KL, and GH. QC, YJL, and XC wrote the manuscript.

Competing interests. The authors declare no competing financial interests.

Acknowledgments. This work is supported by the MOST National Key R&D Program of China (2017YFC0213000, Task 3), the National Natural Science Foundation of China (41875165, 41961134034, 51861135102), the 111 Project of Urban Air Pollution and Health Effects (B20009), The Science and Technology Development Fund, Macau SAR (File no. 0019/2020/A1), University of Macau (File no. MYRG2018-00006-FST). The authors gratefully acknowledge Tong Zhu, Ying Liu, Manjula R. Canagaratna, Andrew Lambe, and Peng Zhe for instrument support and helpful discussion.

References

Arey, J., Obermeyer, G., Aschmann, S. M., Chattopadhyay, S., Cusick, R. D., and Atkinson, R.: Dicarbonyl products of the OH radical-initiated reaction of a series of aromatic hydrocarbons, Environ. Sci. Technol., 43, 683-689, https://doi.org/10.1021/es8019098, 2009.

Atkinson, R.: Atmospheric chemistry of VOCs and NOx, Atmos. Environ., 34, 2063-2101, https://doi.org/https://doi.org/10.1016/S1352-2310(99)00460-4, 2000.

Atkinson, R., and Arey, J.: Atmospheric degradation of volatile organic compounds, Chem. Rev., 103, 4605-4638, https://doi.org/10.1021/cr0206420, 2003.

Berndt, T., Richters, S., Jokinen, T., Hyttinen, N., Kurten, T., Otkjaer, R. V., Kjaergaard, H. G., Stratmann, F., Herrmann, H., Sipila, M., Kulmala, M., and Ehn, M.: Hydroxyl radical-induced formation of highly oxidized organic compounds, Nat. Commun., 7, 13677, https://doi.org/10.1038/ncomms13677, 2016.

https://doi.org/10.5194/acp-2021-201
Preprint. Discussion started: 11 March 2021

Atmospheric Chemistry and Physics Discussions

Bianchi, F., Kurten, T., Riva, M., Mohr, C., Rissanen, M. P., Roldin, P., Berndt, T., Crounse, J. D., Wennberg, P. O., Mentel, T. F., Wildt, J., Junninen, H., Jokinen, T., Kulmala, M., Worsnop, D. R., Thornton, J. A., Donahue, N., Kjaergaard, H. G., and Ehn, M.: Highly oxygenated organic oolecules (HOM) from gas-phase autoxidation involving peroxy radicals: a key contributor to atmospheric aerosol, Chem. Rev., 119, 3472-3509, https://doi.org/10.1021/acs.chemrev.8b00395, 2019.

Birdsall, A. W., Andreoni, J. F., and Elrod, M. J.: Investigation of the role of bicyclic peroxy radicals in the oxidation mechanism of toluene, J. Phys. Chem. A, 114, 10655-10663, https://doi.org/10.1021/jp105467e, 2010.

Birdsall, A. W., and Elrod, M. J.: Comprehensive NO-dependent study of the products of the oxidation of atmospherically relevant aromatic compounds, J. Phys. Chem. A, 115, 5397-5407, https://doi.org/10.1021/jp2010327, 2011.

Brophy, P., and Farmer, D. K.: A switchable reagent ion high resolution time-of-flight chemical ionization mass spectrometer for real-time measurement of gas phase oxidized species: characterization from the 2013 southern oxidant and aerosol study, Atmos. Meas. Tech., 8, 2945-2959, https://doi.org/10.5194/amt-8-2945-2015, 2015.

Calvert, J. G., Atkinson, R., Becker, K. H., Kamens, R. M., Seinfeld, J. H., Wallington, T. J., and Yarwood, G. Y.: The mechanisms of atmospheric oxidation of aromatic hydrocarbons, Oxford University Press, New York, 2002.

Calvert, J. G., Orlando, J. J., Stockwell, W. R., and Wallington, T. J.: The mechanisms of reactions influencing atmospheric ozone, Oxford University Press, New York, 2015.

Cheng, X., Chen, Q., Li, Y., Huang, G., Liu, Y., Lu, S., Zheng, Y., Qiu, W., Lu, K., Qiu, X., Bianchi, F., Yan, C., Yuan, B., Shao, M., Wang, Z., Canagaratna, M. R., Zhu, T., Wu, Y., and Zeng, L.: Secondary production of gaseous nitrated phenols in polluted urban environments, In review., 2020.

Crounse, J. D., Nielsen, L. B., Jørgensen, S., Kjaergaard, H. G., and Wennberg, P. O.: Autoxidation of organic compounds in the atmosphere, J. Phys. Chem. Lett., 4, 3513-3520, https://doi.org/10.1021/jz4019207, 2013.

Ehn, M., Thornton, J. A., Kleist, E., Sipila, M., Junninen, H., Pullinen, I., Springer, M., Rubach, F., Tillmann, R., Lee, B., Lopez-Hilfiker, F., Andres, S., Acir, I. H., Rissanen, M., Jokinen, T., Schobesberger, S., Kangasluoma, J., Kontkanen, J., Nieminen, T., Kurten, T., Nielsen, L. B., Jorgensen, S., Kjaergaard, H. G., Canagaratna, M., Dal Maso, M., Berndt, T., Petaja, T., Wahner, A., Kerminen, V. M., Kulmala, M., Worsnop, D. R., Wildt, J., and Mentel, T. F.: A large source of low-volatility secondary organic aerosol, Nature, 506, 476-479, https://doi.org/10.1038/nature13032, 2014.

Gallimore, P. J., Achakulwisut, P., Pope, F. D., Davies, J. F., Spring, D. R., and Kalberer, M.: Importance of relative humidity in the oxidative ageing of organic aerosols: case study of the ozonolysis of maleic acid aerosol, Atmos. Chem. Phys., 11, 12181-12195, https://doi.org/10.5194/acp-11-12181-2011, 2011.

Garmash, O., Rissanen, M. P., Pullinen, I., Schmitt, S., Kausiala, O., Tillmann, R., Zhao, D., Percival, C., Bannan, T. J., Priestley, M., Hallquist, Å. M., Kleist, E., Kiendler-Scharr, A., Hallquist, M., Berndt, T., McFiggans, G., Wildt, J., Mentel, T. F., and Ehn, M.: Multi-generation OH oxidation as a source for highly oxygenated organic molecules from aromatics, Atmos. Chem. Phys., 20, 515-537, https://doi.org/10.5194/acp-20-515-2020, 2020.

https://doi.org/10.5194/acp-2021-201
Preprint. Discussion started: 11 March 2021

Atmospheric Chemistry and Physics Discussions

Gowda, D., and Kawamura, K.: Seasonal variations of low molecular weight hydroxy-dicarboxylic acids and oxaloacetic acid in remote marine aerosols from Chichijima Island in the western North Pacific (December 2010–November 2011), Atmos. Res., 204, 128-135, https://doi.org/https://doi.org/10.1016/j.atmosres.2018.01.007, 2018.

Heinritzi, M., Simon, M., Steiner, G., Wagner, A. C., Kurten, A., Hansel, A., and Curtius, J.: Characterization of the mass-dependent transmission efficiency of a CIMS, Atmos. Meas. Tech., 9, 1449-1460, https://doi.org/10.5194/amt-9-1449-2016, 2016.

Huang, G., Liu, Y., Shao, M., Li, Y., Chen, Q., Zheng, Y., Wu, Z., Liu, Y., Wu, Y., Hu, M., Li, X., Lu, S., Wang, C., Liu, J., Zheng, M., and Zhu, T.: Potentially important contribution of gas-phase oxidation of naphthalene and methylnaphthalene to secondary organic aerosol during haze events in Beijing, Environ. Sci. Technol., 53, 1235-1244, https://doi.org/10.1021/acs.est.8b04523, 2019.

Hyttinen, N., Kupiainen-Määttä, O., Rissanen, M. P., Muuronen, M., Ehn, M., and Kurtén, T.: Modeling the charging of highly oxidized cyclohexene ozonolysis products using nitrate-based chemical ionization, J. Phys. Chem. A, 119, 6339-6345, https://doi.org/10.1021/acs.jpca.5b01818, 2015.

IUPAC: http://iupac.pole-ether.fr, 2008.

Jenkin, M. E., Saunders, S. M., Wagner, V., and Pilling, M. J.: Protocol for the development of the Master Chemical Mechanism, MCM v3 (Part B): tropospheric degradation of aromatic volatile organic compounds, Atmos. Chem. Phys., 3, 181-193, https://doi.org/10.5194/acp-3-181-2003, 2003.

Jenkin, M. E., Valorso, R., Aumont, B., and Rickard, A. R.: Estimation of rate coefficients and branching ratios for reactions of organic peroxy radicals for use in automated mechanism construction, Atmos. Chem. Phys., 19, 7691-7717, https://doi.org/10.5194/acp-19-7691-2019, 2019.

Jokinen, T., Sipilä, M., Junninen, H., Ehn, M., Lönn, G., Hakala, J., Petäjä, T., Mauldin Iii, R. L., Kulmala, M., and Worsnop, D. R.: Atmospheric sulphuric acid and neutral cluster measurements using CI-APi-TOF, Atmos. Chem. Phys., 12, 4117-4125, https://doi.org/10.5194/acp-12-4117-2012, 2012.

Kirchner, F., Mayer-Figge, A., Zabel, F., and Becker, K. H.: Thermal stability of peroxynitrates, Int. J. Chem. Kinet., 31, 127-144, https://doi.org/10.1002/(sici)1097-4601(1999)31:2<127::aid-kin6>3.0.co;2-l, 1999.

Lambe, A., Massoli, P., Zhang, X., Canagaratna, M., Nowak, J., Daube, C., Yan, C., Nie, W., Onasch, T., Jayne, J., Kolb, C., Davidovits, P., Worsnop, D., and Brune, W.: Controlled nitric oxide production via O(1-D) + N2O reactions for use in oxidation flow reactor studies, Atmos. Meas. Tech., 10, 2283-2298, https://doi.org/10.5194/amt-10-2283-2017, 2017.

Lambe, A. T., Ahern, A. T., Williams, L. R., Slowik, J. G., Wong, J. P. S., Abbatt, J. P. D., Brune, W. H., Ng, N. L., Wright, J. P., Croasdale, D. R., Worsnop, D. R., Davidovits, P., and Onasch, T. B.: Characterization of aerosol photooxidation flow reactors: heterogeneous oxidation, secondary organic aerosol formation and cloud condensation nuclei activity measurements, Atmos. Meas. Tech., 4, 445-461, https://doi.org/10.5194/amt-4-445-2011, 2011.

Li, L. J., Tang, P., Nakao, S., and Cocker, D. R.: Impact of molecular structure on secondary organic aerosol formation from aromatic hydrocarbon photooxidation under low-NOx conditions, Atmos. Chem. Phys., 16, 10793-10808, https://doi.org/10.5194/acp-16-10793-2016, 2016.

Mehra, A., Wang, Y., Krechmer, J. E., Lambe, A., Majluf, F., Morris, M. A., Priestley, M., Bannan, T. J., Bryant, D. J., Pereira, K. L., Hamilton, J. F., Rickard, A. R., Newland, M. J., Stark, H., Croteau, P., Jayne, J. T., Worsnop, D. R., Canagaratna, M. R., Wang, L., and Coe, H.: Evaluation of the chemical composition of gas- and particle-phase products of aromatic oxidation, Atmos. Chem. Phys., 20, 9783-9803, https://doi.org/10.5194/acp-20-9783-2020, 2020.

Mentel, T. F., Springer, M., Ehn, M., Kleist, E., Pullinen, I., Kurtén, T., Rissanen, M., Wahner, A., and Wildt, J.: Formation of highly oxidized multifunctional compounds: autoxidation of peroxy radicals formed in the ozonolysis of alkenes – deduced from structure–product relationships, Atmos. Chem. Phys., 15, 6745-6765, https://doi.org/10.5194/acp-15-6745-2015, 2015.

Molteni, U., Bianchi, F., Klein, F., El Haddad, I., Frege, C., Rossi, M. J., Dommen, J., and Baltensperger, U.: Formation of highly oxygenated organic molecules from aromatic compounds, Atmos. Chem. Phys., 18, 1909-1921, https://doi.org/10.5194/acp-18-1909-2018, 2018.

Molteni, U., Simon, M., Heinritzi, M., Hoyle, C. R., Bernhammer, A.-K., Bianchi, F., Breitenlechner, M., Brilke, S., Dias, A., Duplissy, J., Frege, C., Gordon, H., Heyn, C., Jokinen, T., Kuerten, A., Lehtipalo, K., Makhmutov, V., Petaja, T., Pieber, S. M., Praplan, A. P., Schobesberger, S., Steiner, G., Stozhkov, Y., Tome, A., Trostl, J., Wagner, A. C., Wagner, R., Williamson, C., Yan, C., Baltensperger, U., Curtius, J., Donahue, N. M., Hansel, A., Kirkby, J., Kulmala, M., Worsnop, D. R., and Dommen, J.: Formation of highly oxygenated organic molecules from α-pinene ozonolysis: chemical characteristics, mechanism, and kinetic model development, ACS Earth Space Chem., 3, 873-883, https://doi.org/10.1021/acsearthspacechem.9b00035, 2019.

Nah, T., Sanchez, J., Boyd, C. M., and Ng, N. L.: Photochemical aging of α-pinene and β-pinene secondary organic aerosol formed from nitrate radical oxidation, Environ. Sci. Technol., 50, 222-231, https://doi.org/10.1021/acs.est.5b04594, 2016.

Newland, M. J., Bryant, D. J., Dunmore, R. E., Bannan, T. J., Acton, W. J. F., Langford, B., Hopkins, J. R., Squires, F. A., Dixon, W., Drysdale, W. S., Ivatt, P. D., Evans, M. J., Edwards, P. M., Whalley, L. K., Heard, D. E., Slater, E. J., Woodward-Massey, R., Ye, C., Mehra, A., Worrall, S. D., Bacak, A., Coe, H., Percival, C. J., Hewitt, C. N., Lee, J. D., Cui, T., Surratt, J. D., Wang, X., Lewis, A. C., Rickard, A. R., and Hamilton, J. F.: Low-NO atmospheric oxidation pathways in a polluted megacity, Atmos. Chem. Phys., 21, 1613-1625, https://doi.org/10.5194/acp-21-1613-2021, 2021.

Ng, N. L., Kroll, J. H., Chan, A. W. H., Chhabra, P. S., Flagan, R. C., and Seinfeld, J. H.: Secondary organic aerosol formation from m-xylene, toluene, and benzene, Atmos. Chem. Phys., 7, 3909-3922, https://doi.org/10.5194/acp-7-3909-2007, 2007.

Noda, J., Volkamer, R., and Molina, M. J.: Dealkylation of Alkylbenzenes: A Significant Pathway in the Toluene, o-, m-, p-Xylene plus OH Reaction, J. Phys. Chem. A, 113, 9658-9666, https://doi.org/10.1021/jp901529k, 2009.

Orlando, J. J., Tyndall, G. S., and Wallington, T. J.: The atmospheric chemistry of alkoxy radicals, Chem. Rev., 103, 4657-4690, https://doi.org/10.1021/cr020527p, 2003.

Peng, Z., Palm, B. B., Day, D. A., Talukdar, R. K., Hu, W. W., Lambe, A. T., Brune, W. H., and Jimenez, J. L.: Model evaluation of new techniques for maintaining high-NO conditions in oxidation flow reactors for the study of OH-initiated atmospheric chemistry, ACS Earth Space Chem., 2, 72-86, https://doi.org/10.1021/acs.earth.spacechem.7b00070, 2018.

Rissanen, M. P.: NO2 suppression of autoxidation-inhibition of gas-phase highly oxidized dimer product formation, ACS Earth Space Chem., 2, 1211-1219, https://doi.org/10.1021/acsearthspacechem.8b00123, 2018.

Sarnela, N., Jokinen, T., Duplissy, J., Yan, C., Nieminen, T., Ehn, M., Schobesberger, S., Heinritzi, M., Ehrhart, S., Lehtipalo, K., Tröstl, J., Simon, M., Kürten, A., Leiminger, M., Lawler, M. J., Rissanen, M. P., Bianchi, F., Praplan, A. P., Hakala, J., Amorim, A., Gonin, M., Hansel, A., Kirkby, J., Dommen, J., Curtius, J., Smith, J. N., Petäjä, T., Worsnop, D. R., Kulmala, M., Donahue, N. M., and Sipilä, M.: Measurement–model comparison of stabilized Criegee intermediate and highly oxygenated molecule production in the CLOUD chamber, Atmos. Chem. Phys., 18, 2363-2380, https://doi.org/10.5194/acp-18-2363-2018, 2018.

Sato, K., Takami, A., Kato, Y., Seta, T., Fujitani, Y., Hikida, T., Shimono, A., and Imamura, T.: AMS and LC/MS analyses of SOA from the photooxidation of benzene and 1,3,5-trimethylbenzene in the presence of NOx: effects of chemical structure on SOA aging, Atmos. Chem. Phys., 12, 4667-4682, https://doi.org/10.5194/acp-12-4667-2012, 2012.

Schwantes, R. H., Schilling, K. A., McVay, R. C., Lignell, H., Coggon, M. M., Zhang, X., Wennberg, P. O., and Seinfeld, J. H.: Formation of highly oxygenated low-volatility products from cresol oxidation, Atmos. Chem. Phys., 17, 3453-3474, https://doi.org/10.5194/acp-17-3453-2017, 2017.

Seinfeld, J. H., and Pandis, S. N.: Atmospheric Chemistry and Physics: From Air Pollution to Climate Change, Third Edition, John Wiley & Sons, Inc., Hoboken, New Jersey, 2016.

Tsiligiannis, E., Hammes, J., Salvador, C. M., Mentel, T. F., and Hallquist, M.: Effect of NOx on 1,3,5-trimethylbenzene (TMB) oxidation product distribution and particle formation, Atmos. Chem. Phys., 19, 15073-15086, https://doi.org/10.5194/acp-19-15073-2019, 2019.

Wang, L. M., Wu, R. R., and Xu, C.: Atmospheric oxidation mechanism of benzene. fates of alkoxy radical intermediates and revised mechanism, J. Phys. Chem. A, 117, 14163-14168, https://doi.org/10.1021/jp4101762, 2013.

Wang, M., Chen, D., Xiao, M., Ye, Q., Stolzenburg, D., Hofbauer, V., Ye, P., Vogel, A. L., Mauldin, R. L., Amorim, A., Baccarini, A., Baumgartner, B., Brilke, S., Dada, L., Dias, A., Duplissy, J., Finkenzeller, H., Garmash, O., He, X., Hoyle, C. R., Kim, C., Kvashnin, A., Lehtipalo, K., Fischer, L., Molteni, U., Petäjä, T., Pospisilova, V., Quéléver, L. L. J., Rissanen, M. P., Simon, M., Tauber, C., Tomé, A., Wagner, A. C., Weitz, L., Volkamer, R., Winkler, P. M., Kirkby, j., Worsnop, D. R., Kulmala, M., Baltensperger, U., Dommen, J., El Haddad, I., and Donahue, N. M.: Photo-oxidation of aromatic hydrocarbons produces low-volatility organic compounds, Environ. Sci. Technol., https://doi.org/10.1021/acs.est.0c02100, 2020.

Wang, S., Wu, R., Berndt, T., Ehn, M., and Wang, L.: Formation of highly oxidized radicals and multifunctional products from the atmospheric oxidation of alkylbenzenes, Environ. Sci. Technol., 51, 8442-8449, https://doi.org/10.1021/acs.est.7b02374, 2017.

Wang, Y., Mehra, A., Krechmer, J. E., Yang, G., Hu, X., Lu, Y., Lambe, A., Canagaratna, M., Chen, J., Worsnop, D., Coe, H., and Wang, L.: Oxygenated products formed from OH-initiated reactions of trimethylbenzene: autoxidation and accretion, Atmos. Chem. Phys., 20, 9563-9579, https://doi.org/10.5194/acp-20-9563-2020, 2020.

Wu, R., Pan, S., Li, Y., and Wang, L.: Atmospheric oxidation mechanism of toluene, J. Phys. Chem. A, 118, 4533-4547, https://doi.org/10.1021/jp500077f, 2014.

Xu, L., Møller, K. H., Crounse, J. D., Kjaergaard, H. G., and Wennberg, P. O.: New insights into the radical chemistry and product distribution in the OH-initiated oxidation of benzene, Environ. Sci. Technol., 54, 13467-13477, https://doi.org/10.1021/acs.est.0c04780, 2020.

Yu, J. Z., and Jeffries, H. E.: Atmospheric photooxidation of alkylbenzenes-II. Evidence of formation of epoxide intermediates, Atmos. Environ., 31, 2281-2287, https://doi.org/10.1016/s1352-2310(97)88637-2, 1997.

Yu, J. Z., Jeffries, H. E., and Sexton, K. G.: Atmospheric photooxidation of alkylbenzenes-I. Carbonyl product analyses, Atmos. Environ., 31, 2261-2280, https://doi.org/10.1016/s1352-2310(97)00011-3, 1997.

Zaytsev, A., Koss, A. R., Breitenlechner, M., Krechmer, J. E., Nihill, K. J., Lim, C. Y., Rowe, J. C., Cox, J. L., Moss, J., Roscioli, J. R., Canagaratna, M. R., Worsnop, D. R., Kroll, J. H., and Keutsch, F. N.: Mechanistic study of the formation of ring-retaining and ring-opening products from the oxidation of aromatic compounds under urban atmospheric conditions, Atmos. Chem. Phys., 19, 15117-15129, https://doi.org/10.5194/acp-19-15117-2019, 2019.

Zhao, Y., Thornton, J. A., and Pye, H. O. T.: Quantitative constraints on autoxidation and dimer formation from direct probing of monoterpene-derived peroxy radical chemistry, Proc. Natl. Acad. Sci. U. S. A., 115, 12142-12147, https://doi.org/10.1073/pnas.1812147115, 2018.

Zheng, Y., Cheng, X., Liao, K. R., Li, Y. W., Li, Y. J., Hu, W. W., Liu, Y., Zhu, T., Chen, S. Y., Zeng, L. M., Worsnop, D., Chen, Q., and Huang, R. J.: Characterization of anthropogenic organic aerosols by TOF-ACSM with the new capture vaporizer, Atmos. Meas. Tech., 13, 2457-2472, https://doi.org/10.5194/amt-13-2457-2020, 2020.

Ziemann, P. J., and Atkinson, R.: Kinetics, products, and mechanisms of secondary organic aerosol formation, Chem. Soc. Rev., 41, 6582-6605, https://doi.org/10.1039/C2CS35122F, 2012.

https://doi.org/10.5194/acp-2021-201
Preprint. Discussion started: 11 March 2021

List of Figures

Figure 1. Mass spectra of HOM products measured by the NO_3^--TOF-CIMS for Exp. #2, #11, #16, and #26 in Table S1. (a): benzene, OFR254-5; (b) benzene, OFR254-5-iN_2O4.4; (c): toluene, OFR254-5; (d) toluene, OFR254-5-iN_2O4.4. The reagent ion NO_3^- is omitted from the molecular formulas, whereas the *m*/*z* values refer to the mass-to-charge ratios of the fitted ions with NO_3^-. The relative intensities of ions having $m/z \geq 300$ are multiplied by 10.

Figure 2. Concentrations of fragmented, closed-shell, open-shell and dimeric products formed by benzene and toluene oxidation under low-NO_x conditions (OFR254-5) at various OH exposures. For benzene oxidation, both of *x* and *y* are 6. For toluene oxidation, *x* is 7 and *y* is 8. BPR: bicyclic peroxy radical; HP: hydroperoxide; -C=O: carbonyl; -OH: alcohol.

Figure 3. Concentrations and relative contributions of closed-shell products formed by benzene and toluene oxidation under low-NO_x conditions (OFR254-5) at various OH exposures. For benzene oxidation, both of *x* and *y* are 6. For toluene oxidation, *x* is 7 and *y* is 8.

Figure 4. Concentrations of fragmented, closed-shell, open-shell, dimeric and nitrogen-containing products formed by benzene and toluene oxidation under high-NO_x conditions (OFR254-5-iN_2O1.1/4.4) at various [NO_x]:[HO_2] levels. Data for OFR254-5-iN_2O1.1 experiments were averaged and shown as the first data point in each panel. For benzene oxidation, both of *x* and *y* are 6. For toluene oxidation, *x* is 7 and *y* is 8.

Figure 5. Kinetic analysis on the formation of nitrogen-containing HOMs. (a): [ROOH]×k_{loss} vs. [RO_2][HO_2]; (b-c) [$RONO_2$]:[ROOH] vs. [NO]:[HO_2]; (d-e) [RC(O)OONO_2]:[ROOH] vs. [NO_2]:[HO_2]. For benzene oxidation, both of *x* and *y* are 6. For toluene oxidation, *x* is 7 and *y* is 8. k_{loss} represents the loss rate of corresponding HOM products in unit of s^{-1}.

https://doi.org/10.5194/acp-2021-201
Preprint. Discussion started: 11 March 2021

Atmospheric Chemistry and Physics
Open Access
EGU
Discussions

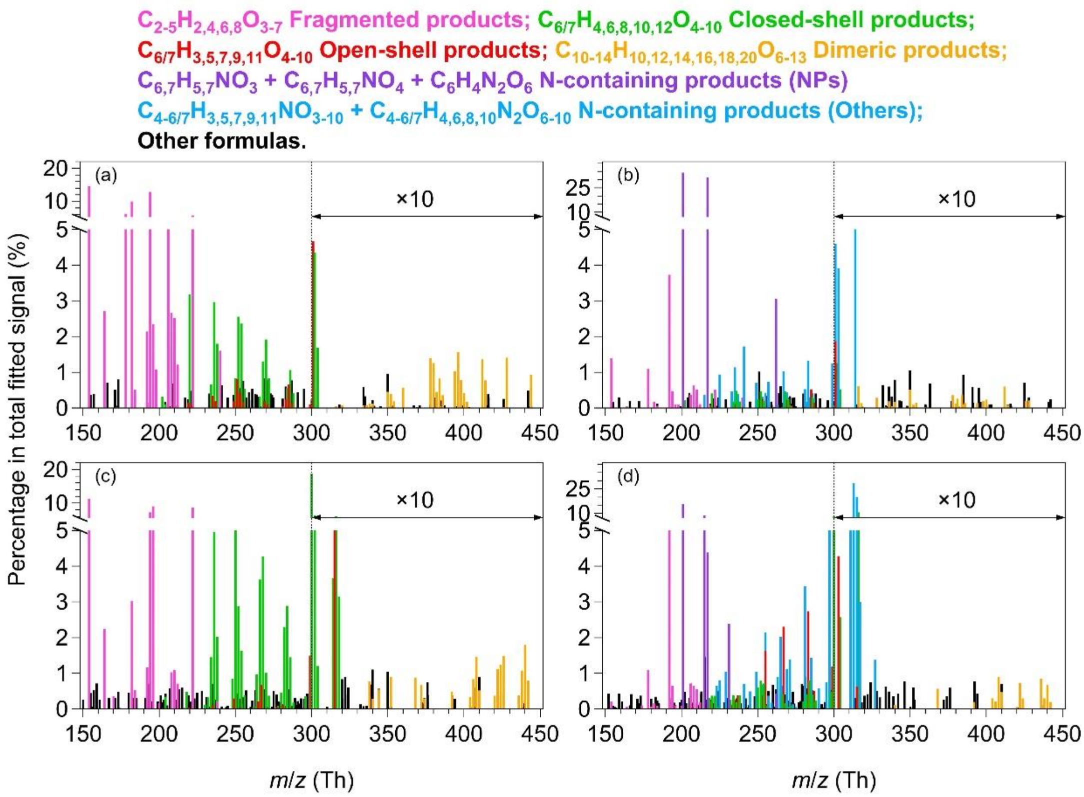

Figure 1

https://doi.org/10.5194/acp-2021-201
Preprint. Discussion started: 11 March 2021

Atmospheric Chemistry and Physics
Open Access
Discussions

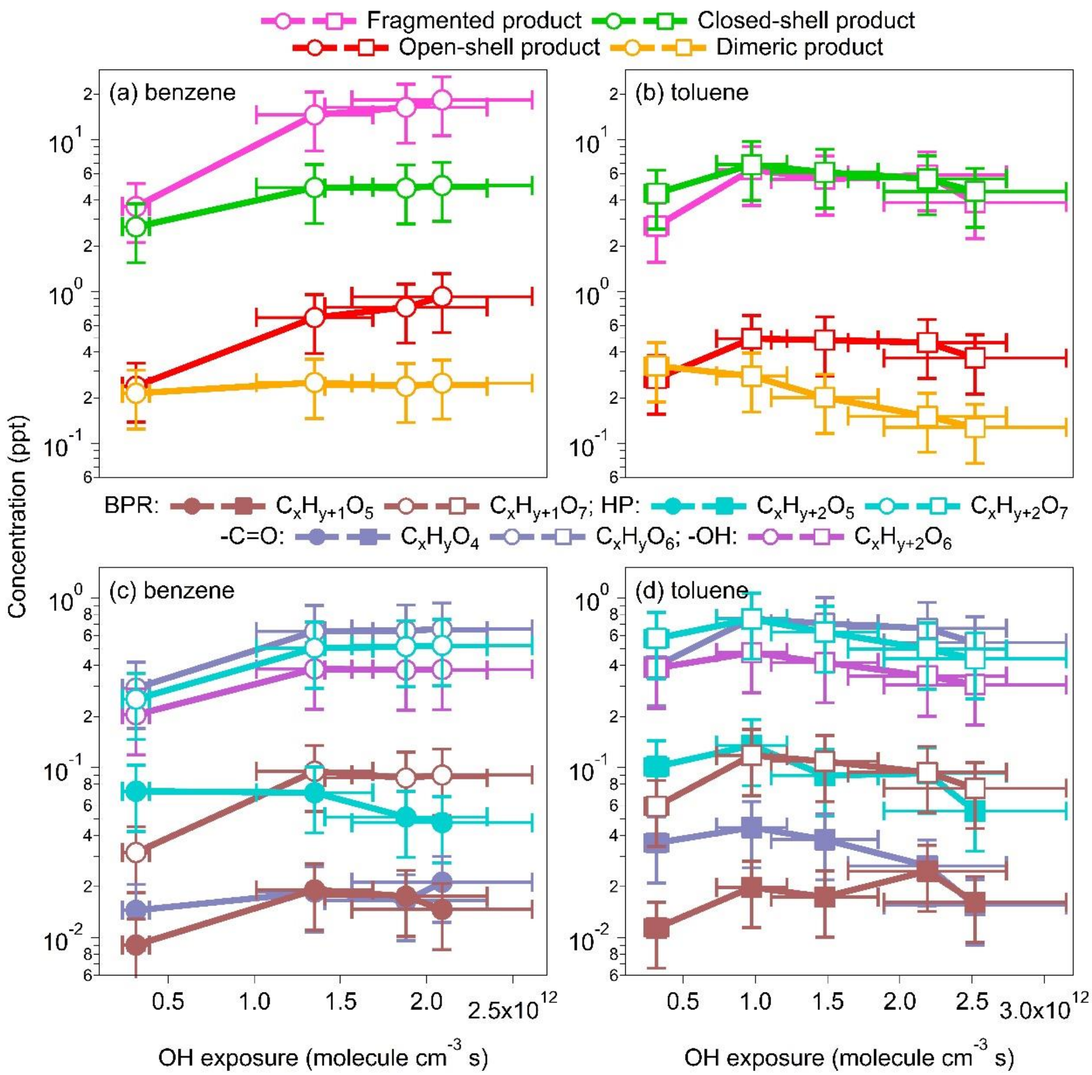

Figure 2

560

https://doi.org/10.5194/acp-2021-201
Preprint. Discussion started: 11 March 2021

Atmospheric Chemistry and Physics
Discussions

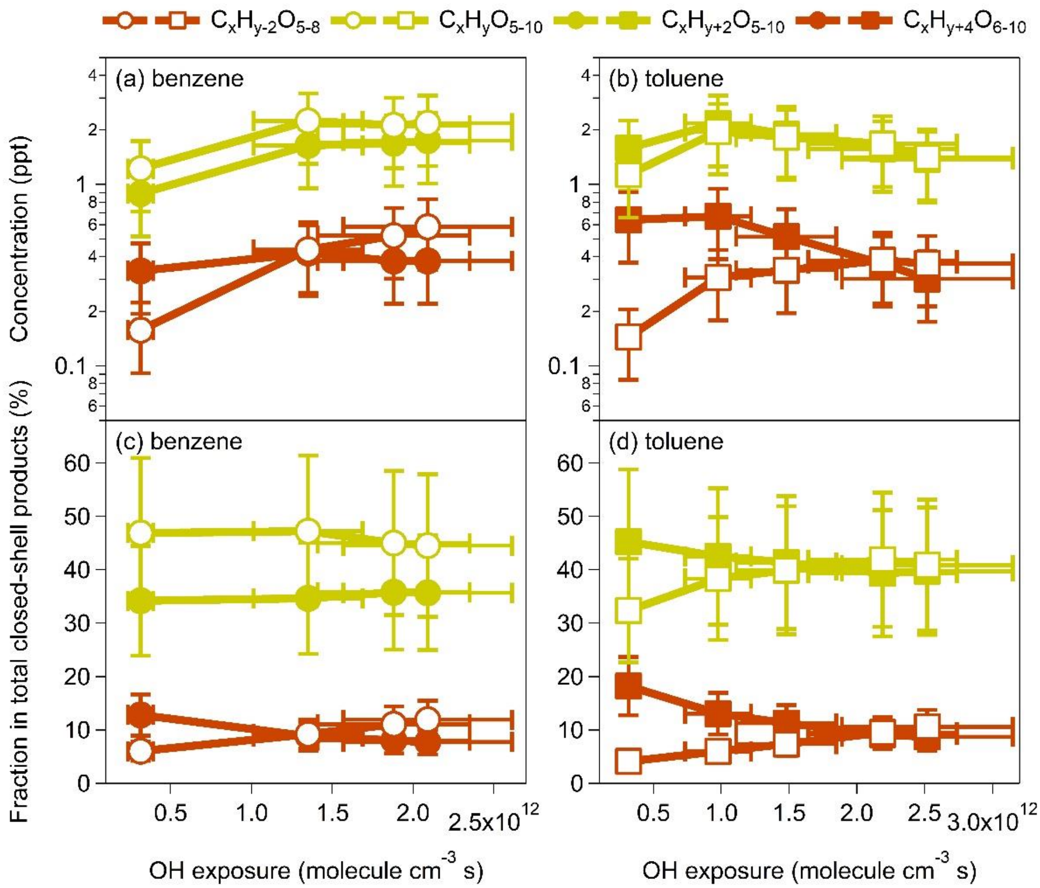

Figure 3

https://doi.org/10.5194/acp-2021-201
Preprint. Discussion started: 11 March 2021

Atmospheric Chemistry and Physics
Open Access
EGU
Discussions

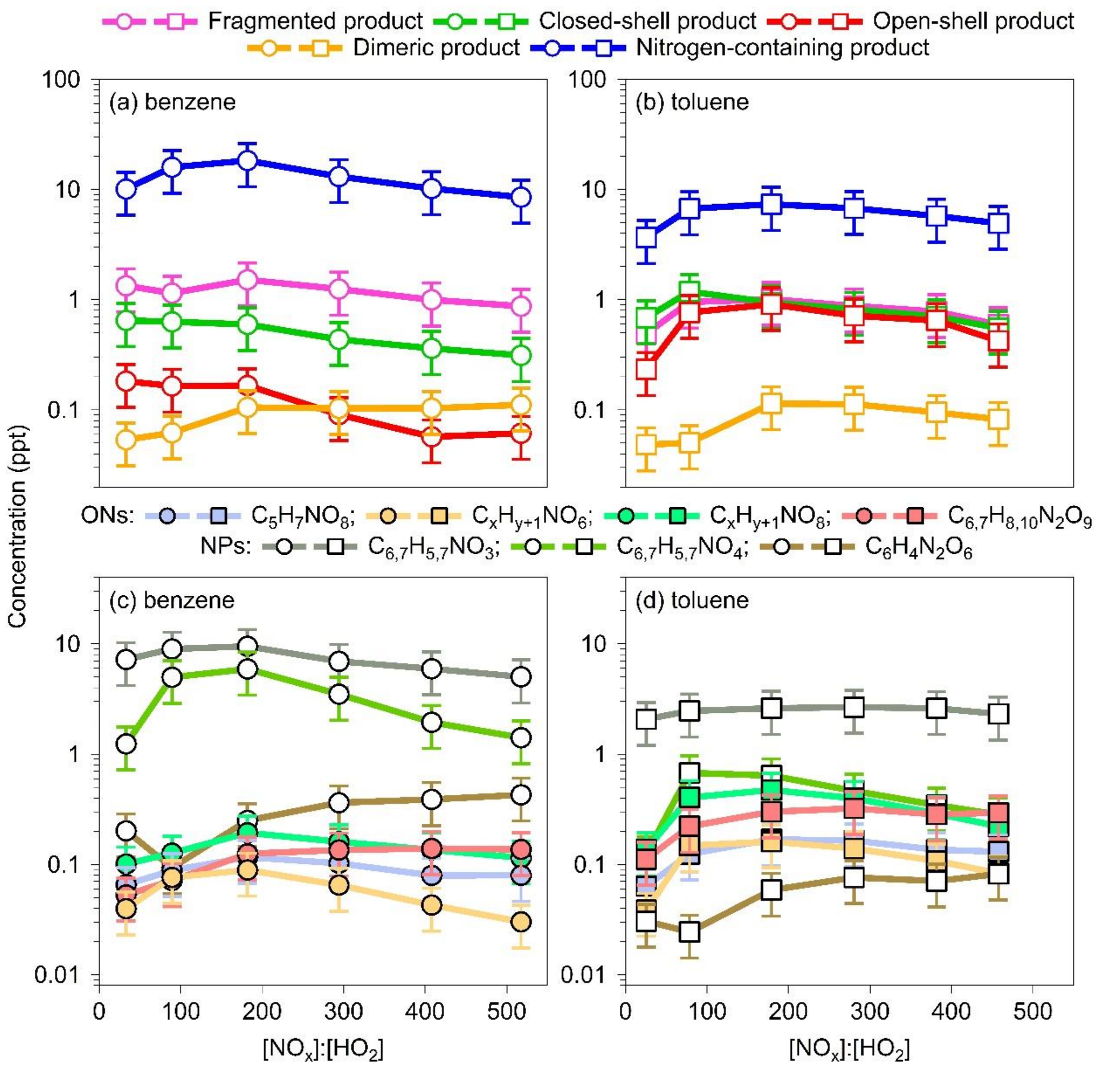

Figure 4

https://doi.org/10.5194/acp-2021-201
Preprint. Discussion started: 11 March 2021

Atmospheric Chemistry and Physics
Open Access
Discussions

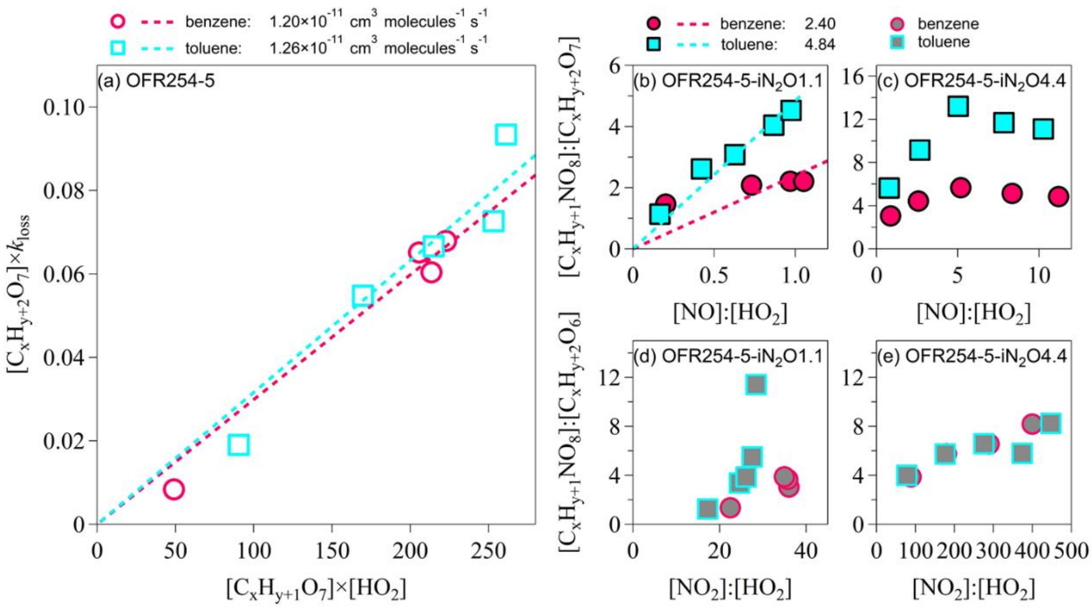

Figure 5